Geothermal Energy

RESEARCH Open Access

Laboratory tests simulating corrosion in geothermal power plants: influence of service conditions

Ana Vallejo Vitaller[1*], Ueli M. Angst[1] and Bernhard Elsener[1,2]

*Correspondence:
ana.vallejo@ethz.ch
[1] Institute for Building Materials (IfB), ETH Zurich, Stefano-Franscini-Platz 3, 8093 Zurich, Switzerland
Full list of author information is available at the end of the article

Abstract

One of the main challenges associated with the operation and maintenance of binary geothermal power plants is the degradation of construction materials. In this sense, it is crucial to apply appropriate preventive maintenance in critical components (such as the wellheads, heat exchangers, or pipes), while reducing shutdown times. Based on electrochemical measurements performed in an autoclave corrosion testing setup, we studied the corrosion mechanism of API L80 steel grade as a function of operational and/or maintenance procedures. We used a test fluid representative for a site in Switzerland, but the main observations made may be applicable in a wider context. We found that changes in the fluid temperature (from 200 to 100 °C) or temporary oxygen ingress significantly influenced the corrosion behavior of this carbon steel and increased its corrosion rate (from approx. 20 µm/year to > 120 µm/year). After a few days, the corrosion rate was found to decrease and stabilize around values of 50–70 µm/year, as a result of a porous corrosion product layer formed on the metal surface (approx. 250 µm thick). Electrochemical impedance spectroscopy indicated an increase in capacitance of the double layer over time, most likely due to an increase in the effective surface area of the steel sample, as a consequence of surface roughening due to corrosion. The results from this study may be implemented in the design and operation of future power plants in Switzerland and elsewhere to ensure reliable and cost-effective energy production from geothermal resources.

Keywords: Geothermal installations, Operational issues, Oxygen, Fluid temperature

Introduction

Geothermal energy has a large potential for becoming part of the future worldwide energy portfolio, considering its steady growth over the past decades (Lund and Boyd 2016; Dickson and Fanelli 2013; Barbier 2002). In Switzerland, the future action plans, referred to as "Energy strategy 2050", include the development of sustainable and renewable electricity production, where approximately 4–5 TWh/year will be from deep geothermal resources (Swiss Federal Office of Energy, kein Datum; Hirschberg and Wiemer 2015). The production of deep geothermal energy by means of enhanced geothermal systems (EGS) shows many advantages, such as autonomy, no cost for the resources, and permanent availability. However, there are challenging aspects that refer to the

Journal : BMCOne 40517 | Dispatch : 9-3-2020 | Pages : 17
Article No : 163 | ☐ LE | ☐ TYPESET
MS Code : | ☑ CP | ☑ DISK

accessibility and exploitation of the resources as well as to the long-term durability of the construction materials of the power plant components (Olasolo et al. 2016; Lu 2018).

Regardless of the geothermal energy potential, operational issues in geothermal installations might act as a barrier to reliable and safe energy production (Schreiber et al. 2016). Among these operational issues, corrosion represents a major cause for the degradation of metallic materials and is mostly due to the geothermal fluids enriched in dissolved solids and gases (Karlsdottir 2012; Mundhenk et al. 2013; Nogara and Zarrouk 2018a, b). In general terms, corrosion is defined as the deterioration of a material or its properties due to an electrochemical or chemical reaction with the surrounding environment (Landolt 2007). It occurs spontaneously and can cause dangerous and expensive damage in many types of applications. In a binary geothermal power plant, components, such as the well casings, pipelines, or heat exchangers, generally consist of metallic materials, and thus, subject to corrosion processes (Nogara and Zarrouk 2018a, b; Clark et al. 2010). In Switzerland, previous studies have shown that fluids from regions with optimal conditions for the generation of electricity (and space heating) might lead to corrosion damages in low-alloyed steels, especially at low temperatures (100 °C) (Vallejo Vitaller et al. 2019).

Typically, a geothermal power plant is designed in such a manner that it can smoothly operate during a life span of over 25 years, without requiring extensive maintenance. One of the most important features affecting the design of a power plant is the choice of materials with reasonable economic impact (Ellis and Conover 1981; Iberl et al. 2015; Clark et al. 2010). These construction materials are usually selected based on preliminary feasibility studies—geological, geophysical, and geochemical—that mainly characterizes the reservoir (Ochieng 2014). However, as the properties of the geothermal system might evolve, the operational and maintenance procedures in the power plant need to be adjusted and optimized to avoid substantial material degradation and further costs. This also requires the continuous monitoring of physicochemical parameters, such as pressure, temperature, or fluid chemistry.

A proper power plant operation should ensure maximum efficiency and performance of the process, minimum equipment failures, and maximum safety of the plant and personnel (Ochieng 2014). Furthermore, trouble-free operation requires regular maintenance, including a scheduled replacement of critical equipment. In this regard, reactive and preventive maintenance activities are usually carried out in geothermal power plants to ensure the long-term durability of expensive assets (especially the well casings, downhole pump, and heat exchanger) (Anon. 1994). While reactive maintenance is carried out after a fault with the aim of starting up again the component, preventive maintenance is performed at predetermined intervals (time-based) or based on recommended criteria after inspection (condition-based) to minimize the probability of failure or the degradation of the component (CEN 2010). Predictive maintenance, which is another category of approach, is less common in the geothermal sector, due to the high initial investment; however, operators have shown great interest on its implementation in geothermal installations (Atlason et al. 2014; Sullivan et al. 2010).

The type of maintenance applied should be chosen for each component based on criticality assessment. For instance, it is generally difficult to identify localized corrosion beforehand. If it occurs, the metallic component can fail with no warning and only reactive maintenance is possible. To prevent this, time- and condition-based

Journal : BMCOne 40517 | Dispatch : 9-3-2020 | Pages : 17
Article No : 163 | ☐ LE | ☐ TYPESET
MS Code : | ☑ CP | ☑ DISK

activities can take place in advance in critical and non-critical equipment with the disadvantage of being expensive. Figure 1 schematically depicts an operating power plant where the geothermal fluid is in contact with the metals at temperatures of about 180 °C (at the production wellhead and inlet of the heat exchanger) or 100 °C (e.g., at the outlet of the heat exchanger or injection wellhead). On the other hand, if preventive maintenance is applied in these components taking no precautionary measures, it might lead to a decrease of temperature (down to 90–100 °C) or an ingress of oxygen in the system. These changes in temperature and oxygen concentration may affect the corrosion state of metallic materials, such as the inside of pipes. For instance, it is well known that dissolved oxygen might act as an oxidizing agent and initially accelerate the corrosion process (Landolt 2007; Revie and Uhlig 2008). Moreover, it has recently been shown that a difference in temperature may influence the corrosion conditions (Vallejo Vitaller et al. 2019). In this context, there is a risk that actions meant as "preventive maintenance" may actually enhance corrosion and thus lead to expensive downtimes to the power plant operators.

The aim of this work is to study the impact of time-dependent operational and maintenance procedures on the corrosion of (metallic) equipment in geothermal power plants. These changes might play an important role in the life span of geothermal installations because the environmental conditions are likely to be altered (e.g., a decrease of temperature or ingress of oxygen). For the experimental study, we analyzed the corrosion of metals by means of electrochemical techniques and considered conditions that might be found in deep geothermal energy systems in Switzerland.

Materials and methods

Materials

Synthetic fluid

The composition of the synthetic testing solution used for all experiments is shown in Table 1. This solution composition is within the range of expected geothermal brines

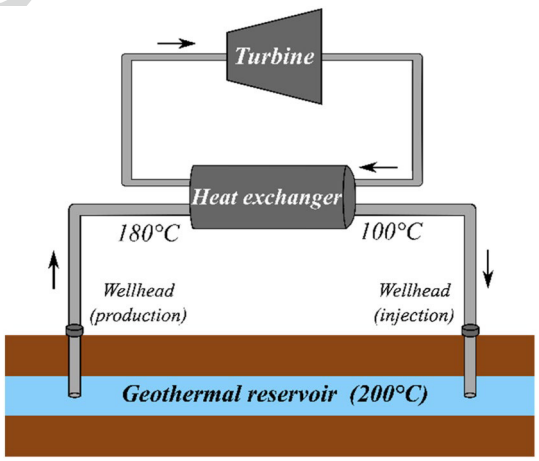

Fig. 1 Schematic drawing of a binary cycle geothermal power plant showing the main components (well casings, wellheads and heat exchanger) that are in contact with the produced and spent geothermal fluid. These components might be subjected to corrosion during the execution of maintenance activities in the power plant

Journal : BMCOne 40517 | Dispatch : 9-3-2020 | Pages : 17
Article No : 163 | ☐ LE | ☐ TYPESET
MS Code : | ☑ CP | ☑ DISK

Table 1 Chemical composition of the testing fluid as prepared in the laboratory at room temperature

	pH	Ca^{2+}	Mg^{2+}	Na^{+}	K^{+}	HCO_3^-	SO_4^{2-}	Cl^-
Synthetic fluid	6.6–7.0	250	45	747	35	1400	900	600

The concentration of the chemical species is in mg/L. The pH values reported here were measured at room temperature immediately after the preparation of the solutions

in Switzerland from sites with optimal conditions for the generation of geothermal energy, based on geographical and geological characteristics (Sonney and Vuataz 2008; Bodmer and Rybach 1985; Wyss and Link 2015). The solution had a near-neutral pH and a high concentration of chlorides. For the tests, the solution was prepared by mixing specific quantities of different stock solutions with ultrapure water at room temperature. The chemicals calcium sulfate (99%), sodium sulfate (> 99.0%), potassium sulfate (> 99.0%), and magnesium sulfate (> 99.5%) were purchased from Sigma-Aldrich GmbH (Buchs, Switzerland). Sodium bicarbonate (ACS, Reag. pH Eur) and sodium chloride (ACS, ISO, Reg. Ph Eur for analysis) were purchased from Merck (Merck KGaA, Darmstadt, Germany), and hydrochloric acid (37%, Reag. Ph. Eur. analytical reagent) from VWR Chemicals.

Steel sample

An API steel grade (L80 Type 1) was used for all the tests. This is a low-alloyed steel commonly employed in the oil and gas industry, mainly for constructing the casing and tubing of wells, and produced according to the specification 5CT of the American Petroleum Institute (API) (API Specification 2005). The chemical composition of this steel is shown in Table 2. The geometry of the steel samples was a cylinder of 20 mm height and 15 mm diameter, with an inner thread of 5 mm to attach it to the sample holder. The surface area of each sample was 1120 ± 50 mm^2. Furthermore, all surfaces were mechanically ground and/or polished with SiC paper (up to 4000 mesh/in.) as well as ultrasonically cleaned with ethanol and dried with compressed air.

Experimental setup

The experiments were carried out in a 1-l autoclave suitable for high temperatures (up to 220 °C) and high pressures (up to 70 bar) featured with several electrochemical tools. A more detailed description of the experimental setup is given in a research paper published by Vallejo Vitaller et al. (2020). Concerning the electrochemical tools, the counter electrode was a Pt plate (5×20 mm^2) and the reference electrode was a silver/silver chloride (Ag/AgCl/Sat. KCl). In addition to the electrochemical cell, other devices were used to carry out potentiometric and potentiodynamic

Table 2 Composition of the tested steel grade (API L80 Type 1), as reported by the manufacturer

Steel sample	wt % (and Fe bal.)										
Composition	C	Si	Mn	Cr	Mo	S	P	Ni	Cu	Al	V
L80 type 1	0.25	0.19	1.02	0.45	0.16	0.004	0.014	0.04	0.02	0.03	0.003

Journal : BMCOne 40517 Dispatch : 9-3-2020 Pages : 17
Article No : 163 ☐ LE ☐ TYPESET
MS Code : ☑ CP ☑ DISK

measurements. These included a potentiostat/galvanostat PGSTAT302N by Metrohm Autolab B.V. (Utrecht, The Netherlands), operated by the Windows software NOVA 2.1.2 (also by Metrohm Autolab), and a Keithley multimeter (model 2701) with a multiplexer (model 7702), connected to a computer for data acquisition through a RJ-45 communication interface. In addition, the potentiostat was used in combination with an isolation transformer to operate it in floating mode and without the risk of creating ground loops in the system.

Methods

Procedure

Figure 2 shows the experimental procedure followed in this study. Initially (phase 1), the testing solutions were de-aerated with nitrogen (purity grade 5.0) for around 1 h to minimize the oxygen concentration. Afterward, nitrogen was injected at a pressure of 15 bar (to prevent degassing of the solutions), and the autoclave was heated up from room temperature to 180 °C. This temperature was maintained for a maximum duration of 2.5 days.

In the second phase (2), the autoclave was cooled down to 90 °C, and the lid opened to allow oxygen of the atmosphere to dissolve in the solution. This condition simulated the maintenance activities carried out in the heat exchanger or in the production's wellhead

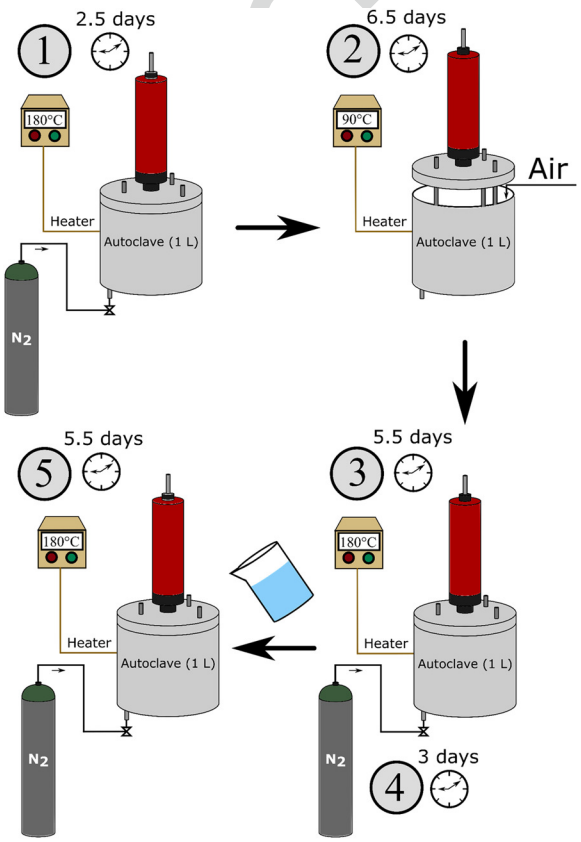

Fig. 2 Experimental procedure followed using the electrochemical setup to mimic the maintenance activities in an operating geothermal power plant

Journal : BMCOne 40517 | Dispatch : 9-3-2020 | Pages : 17
Article No : 163 | ☐ LE | ☐ TYPESET
MS Code : | ☑ CP | ☑ DISK

of an operating power plant. The duration of this phase in our experiments was of max. 6.5 days.

After finishing phase 2, the autoclave was closed again and heated up to 180 °C without de-aerating the solutions (phase 3). The autoclave was kept under these conditions for a maximum of 5.5 days. However, this did not represent the real conditions in an operating power plant, where new geothermal fluid (low in oxygen concentration) coming from the reservoir is immediately produced. Therefore, the subsequent phase in our experiments (4) involved the de-aeration of the solutions to mimic the reducing state of the new geothermal fluid. The duration of the phase 4 was 3 days. The conditions in phase 4 are comparable to phase 1, as the parameters temperature (180 °C) and pressure (15 bar of injected nitrogen) are identical. The chemistry of the fluid is probably still similar to the initial conditions, but it cannot be excluded that it may have changed in the course of the experiment. Thus, to study this potential influence of chemical changes in the exposure fluid, the testing solution inside the vessel was after phase 4 exchanged by a new one of the same composition as in Table 1 and de-aerated. This last phase (phase 5) lasted for around 5.5 days and was carried out at 180 °C with 15 bar of nitrogen initially injected.

In all the phases, a magnetic stirrer was set at a constant speed of 500 rpm. The stirrer was switched off during the electrochemical measurements that were performed at regular times. Furthermore, the heating and cooling rates of the autoclave were 50 °C/h in all cases. Three independent measurements were carried out for the testing solution and the steel grade investigated.

Electrochemical measurements

The potentials of the working electrode (i.e., the open circuit potential, OCP) and of the pH sensor were measured versus the reference electrode and recorded with a Keithley multimeter (model 2701) during all phases (1–5). To evaluate the corrosion state of the exposed metal and to analyze the electrochemical interface metal–electrolyte over the duration of the tests and when changing the exposure conditions (Fig. 2), linear polarization resistance (LPR) and impedance spectroscopy (EIS) measurements were applied using the three-electrode configuration (working, counter, and reference electrodes).

Regarding the polarization resistance measurements, a small external overvoltage of ± 20 mV vs. the OCP was imposed to the working electrode and the resulting current was measured. The sweep rate was 10 mV/min. For the purpose of this work, no IR drop correction was applied. R_p was determined from the slope of the quasi-linear portion of the polarization curves around the OCP. The Stern and Geary equation (Stern and Geary 1957) was used to calculate the corrosion current density (i_{corr}, A/cm^2) as

$$i_{\text{corr}} = \frac{1}{2.303 \cdot \left(\frac{1}{\beta_a} + \frac{1}{|\beta_c|}\right)} \cdot \frac{1}{R_p}, \tag{1}$$

where R_p is the polarization resistance (Ω·cm^2), and β_a and β_c are the anodic and cathodic Tafel slopes, respectively. It is assumed that both Tafel slopes are ± 0.12 V (Jones 1996), given that deviations from these values have limited influence on the results of the LPR technique (Angst et al. 2011). Considering the calculated i_{corr} and

Faraday's first law of electrolysis, the corrosion rate (mm/year) of a metal (e.g., steel) can be determined as

$$\text{Corrosion rate} = K \cdot \frac{i_{\text{corr}} \cdot M_{\text{Fe}}}{z \cdot F \cdot \rho_{\text{Fe}}}, \tag{2}$$

where K is a constant ($3.15 \cdot 10^8$), F is the Faraday constant (96,485 C/mol) and M_{Fe} (g/mol), ρ_{Fe} (g/cm^3), and z refer to the molar mass, density, and oxidation state of iron, respectively.

The electrochemical impedance of the interface solution/metal was determined by imposing an AC signal around the OCP and measuring the resulting AC current. The amplitude of the sinusoidal voltage signal was 10 mV, the frequency (f) range applied was 10 kHz–0.01 Hz, and the step type was logarithmic (7 frequencies/decade). The frequency analyzer calculated the real part Z' and the imaginary part Z'' of the impedance at any frequency. Based on these data, the impedance can be plotted as Nyquist plot (Z'' vs Z') or as Bode plot, where the modulus of the impedance log Z (Ω) and the phase angle (θ) are plotted vs log f. The analysis of the impedance spectra of measurement 3 is presented in "Impedance spectroscopy" section.

Results

pH evolution

Figure 3 shows the pH of the aqueous solution that was tested during three independent measurements inside the autoclave. In addition, the figure indicates the different testing phases 1–5 described in Fig. 2. While the pH of the testing solution hardly changed during the first phase, it increased by around two pH units in the second phase. In the subsequent phases (3, 4, and 5), the pH values remained constant and similar to those measured in phase 1.

Open circuit potential (OCP) evolution

Figure 4 shows the OCP values of the steel specimens that were measured in the autoclave as a function of time. The five phases that correspond to the testing conditions shown in Fig. 2 at different temperatures, pressures, and chemical compositions of the

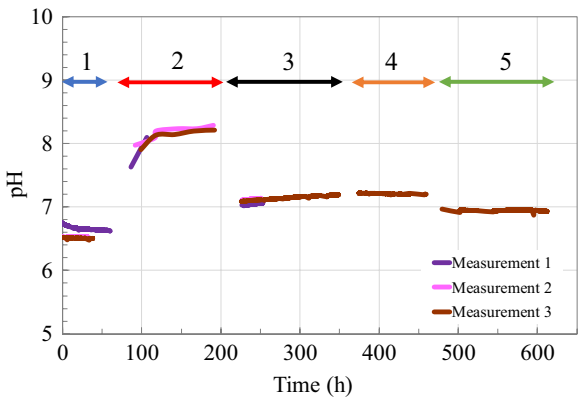

Fig. 3 The pH variation of the aqueous solution measured throughout the five testing phases, which are also indicated in the plot. Three independent measurements were carried out for the testing solution investigated

Journal : BMCOne 40517 | Dispatch : 9-3-2020 | Pages : 17
Article No : 163 | LE | TYPESET
MS Code : | CP | DISK

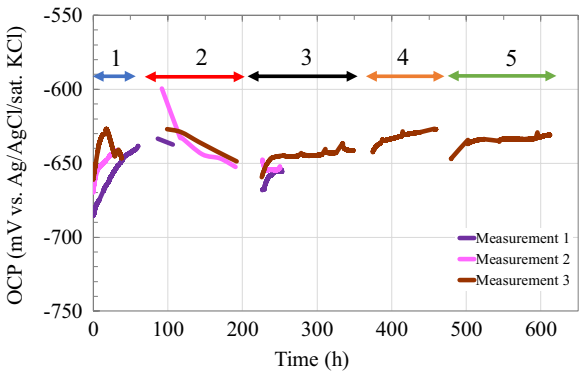

Fig. 4 Open circuit potentials (OCP) of the API steel sample L80 measured over time. Three independent measurements were carried out for the testing solution investigated

fluid are also indicated in this figure. The OCP of the metal samples changed slightly (±50 mV) over the duration of all the phases (from 1 to 5), with a tendency toward more stable values in the course of the experiment.

Corrosion rates obtained with polarization resistance measurements

Figure 5 shows the results of the corrosion rate determined from the R_p measurements. As shown in this figure, the corrosion rate of the metal samples varied significantly over time. Initially, the sample corroded at a rate of around 20 µm/year. However, when the testing conditions were modified by decreasing the temperature and allowing the oxygen to dissolve in the fluid (phase 2), the corrosion rate increased by a factor of more than 5. In phase 3, the corrosion rate decreased until it reached a stable value of approximately 50–70 µm/year that remained constant in both subsequent phases 4 and 5.

Impedance spectroscopy

The impedance spectra obtained during the five phases of the experiment 3 are shown as Nyquist plot (Fig. 6) and as Bode plot (Fig. 7). The other two measurements (1

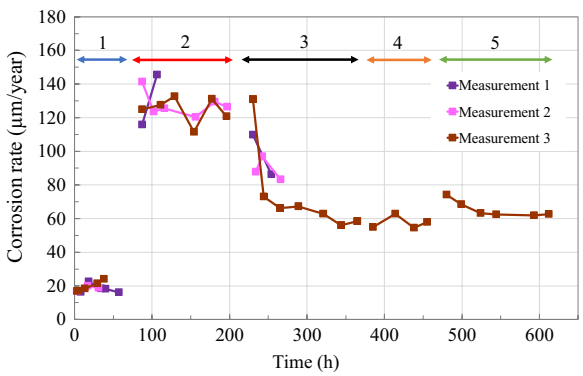

Fig. 5 Corrosion rates (µm/year) obtained from the R_p measurements performed with the API steel grade L80 at two different temperatures (90 and 180 °C) and in the presence and absence of oxygen, as described in Fig. 2. Measurements were repeated three times

Journal : BMCOne 40517 | Dispatch : 9-3-2020 | Pages : 17
Article No : 163 | ☐ LE | ☐ TYPESET
MS Code : | ☑ CP | ☑ DISK

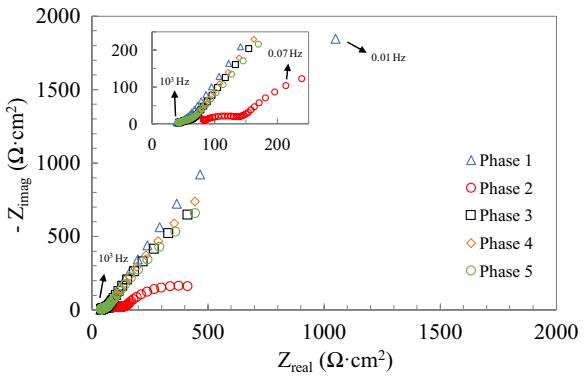

Fig. 6 Electrochemical impedance spectra of the API L80 carbon steel specimens exposed to the testing solution at different temperatures and oxygen concentrations. The spectra shown were obtained during the measurement no. 3

and 2) yielded similar EIS results. A first analysis of the phase angle (Fig. 7b) shows a pronounced maximum at low frequencies (0.01–0.05 Hz) and a small maximum or shoulder at 10–100 Hz. From these two maxima, it can be concluded that two time constants are present in addition to the solution resistance R_s at high frequencies (Fig. 7a). From the Nyquist plot (Fig. 6), it can be observed that no ideal semi-circles are present, and thus, it can be concluded that the capacitance in the two time constants are non-ideal. This non-ideality (due to, e.g., a non-ideal flat surface of the electrode) can be accounted for using constant phase elements' CPE in the equivalent electrical circuit (EEC) assumed for the system as shown in Fig. 8. This EEC is similar to those successfully used in other studies to describe a metal/porous corrosion layer/electrolyte system (Aristia et al. 2019; Bousselmi et al. 1999; Farelas et al. 2010).

Each time constant and element in the equivalent circuit represents a part of the interface electrolyte/porous corrosion product layer/metal. The solution resistance R_s (revealed at high frequencies) is determined by geometry (distance between working electrode and sample) and by the electrolyte conductivity. The first time constant (dominant at high frequencies) is associated to the corrosion product layer formed at the surface (R_{film} and CPE_{film}). The second time constant (dominant at low frequencies) represents the time constant of R_{ct} (charge transfer resistance) and CPE_{dl} (double layer capacitance). With this model, a non-linear regression (curve fitting) was performed on the impedance data. A very good agreement between the experimental data (symbols in Fig. 7) and the curve fit (line in Fig. 7) can be observed. Table 3 provides the values of all the elements, which are in reasonable agreement with those from previous studies, such as Bousselmi et al. (1999), where similar systems were investigated. Note that—in agreement with the very good fit—the relative errors of the individual parameters are relatively small (usually below 30%). The capacitance C (μF·cm^{-2}) of each constant phase element was estimated by means of the following relationship (Brug et al. 1984):

$$C = Q^{1/n} \cdot R^{(1-n)/n} \tag{3}$$

Journal : BMCOne 40517 | Dispatch : 9-3-2020 | Pages : 17
Article No : 163 | LE | TYPESET
MS Code : | CP | DISK

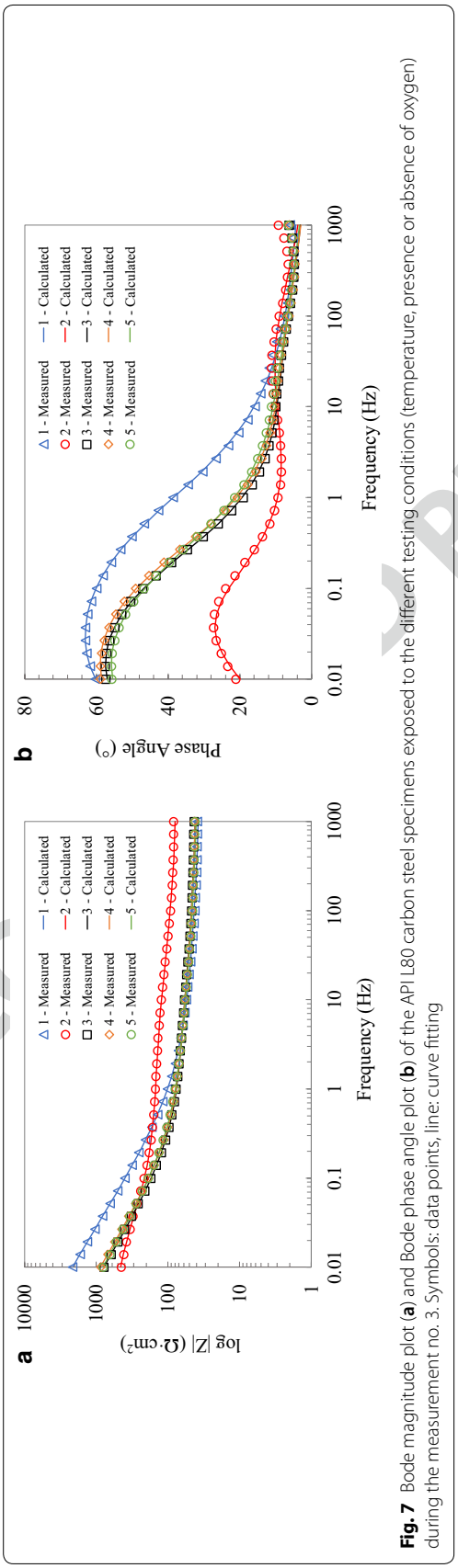

Fig. 7 Bode magnitude plot (**a**) and Bode phase angle plot (**b**) of the API L80 carbon steel specimens exposed to the different testing conditions (temperature, presence or absence of oxygen) during the measurement no. 3. Symbols: data points, line: curve fitting

Journal : **BMCOne 40517** | Dispatch : **9-3-2020** | Pages : **17**
Article No : **163** | ☐ LE | ☐ TYPESET
MS Code : | ☑ CP | ☑ DISK

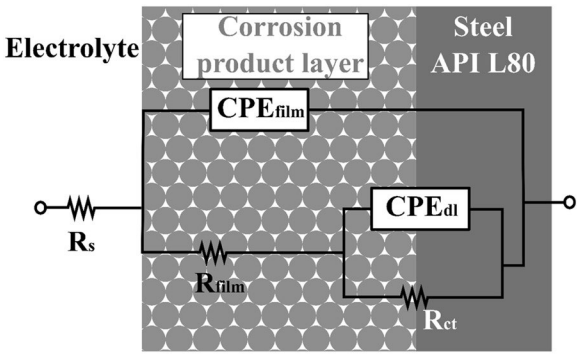

Fig. 8 Equivalent circuit *R*(*Q*(*R*(*QR*))), where the electrolyte, the porous corrosion product layer, and the steel sample API L80 are represented

where Q ($\Omega^{-1}\cdot cm^{-2}\cdot s^{n}$) and n (dimensionless) are parameters of the CPE and R is the resistance (Ω) of the film (R_{film}) or of the double layer (R_{ct}).

It can be noted that the film resistance R_{film} is very small for all experimental conditions (phases 1–5), whereas the charge transfer resistance R_{ct} is in the range of 1000–1900 Ω, except for phase 2 (open to air) where R_{ct} was only about 43 Ω.

Discussion

Evolution of pH and OCP

The pH values of the testing solution remained relatively constant over the whole duration of the measurements, except in the second phase (Fig. 3). The increase of around two pH units in this phase might be an indication of the change of temperature from 180 to 90 °C. However, as shown in previous studies that tested the same type of fluid and steel grade, the pH difference at 100 and 200 °C was of only 0.5 units (Vallejo Vitaller et al. 2019). Thus, this temporary alkalization of the aqueous solution might be due to a change of partial pressure of the gases. Furthermore, the OCP evolution (Fig. 4) showed an insignificant variation over time. Only at the beginning of the second phase, the OCP of the metal sample increased, probably due to a high oxygen concentration.

Corrosion rate as a function of operational conditions

Concerning the results obtained with the polarization resistance measurements, the corrosion rate of the metal sample evolved along the different phases (1–5). The initial corrosion rate of about 20 µm/year is considered a negligible value in this type of applications. In the second phase (Fig. 5), it can be noticed that the corrosion rate increased significantly, namely by a factor of > 5, compared to phase 1. This increase is reasonable considering that oxygen entered the system and the temperature decreased. Moreover, this result is in agreement with previous studies testing the same kind of fluid and metal (Vallejo Vitaller et al. 2019), in which the averaged corrosion rate over 120 h at 100 °C (308 µm/year) was higher than at 200 °C (52 µm/year). Other studies have also evidenced lower corrosion rates toward higher temperatures (> 120 °C) (Mundhenk et al. 2019). In phase 3, the corrosion rate gradually decreased down to approximately 50–70 µm/year. This value remained constant until

Journal : BMCOne 40517 | Dispatch : 9-3-2020 | Pages : 17
Article No : 163 | ☐ LE | ☐ TYPESET
MS Code : | ☑ CP | ☑ DISK

Table 3 Parameters of the components of the equivalent circuit $R(Q(R(QR)))$ for the steel sample in the experimental phases 1, 2, 3, 4, and 5

Phase	R_s ($\Omega \cdot cm^2$)	Error (%)	C_{film} (F)	Error (%)	n_{film}	Error (%)	R_{film} ($\Omega \cdot cm^2$)	Error (%)	C_{dl} (F)	Error (%)	n_{dl}	Error (%)	R_{ct} ($\Omega \cdot cm^2$)	Error (%)	χ^2
1	38	1.0	4.2E−08	30.5	0.74	6.8	30	17.9	1.1E−06	13.5	0.76	2.6	20,482	10.4	7.4E−05
2	76	1.0	1.5E−08	8.3	0.64	2.8	75	3.0	2.7E−06	1.2	0.76	1.2	473	2.0	6.9E−05
3	41	0.5	6.3E−08	7.2	0.59	2.3	37	4.3	2.9E−06	2.9	0.79	1.1	11,506	21.1	2.1E−05
4	41	0.5	6.3E−08	8.5	0.61	2.5	36	5.1	2.8E−06	3.5	0.79	1.2	15,169	25.4	2.6E−05
5	40	0.6	6.9E−08	10.2	0.60	3.1	39	6.9	3.2E−06	4.8	0.76	1.6	12,331	26.1	3.0E−05

Journal : BMCOne 40517 | Dispatch : 9-3-2020 | Pages : 17
Article No : 163 | ☐ LE | ☐ TYPESET
MS Code : | ☑ CP | ☑ DISK

Table 4 R_p values (Ω cm^2) calculated from the R_p measurements and from the impedance spectroscopy results ($R_p = R_{film} + R_{ct}$)

Phase	Electrochemical technique	
	LPR	EIS
1	9262	20,515 ± 2134
2	605	550 ± 11
3	3553	11,539 ± 2442
4	4367	15,202 ± 3861
5	3597	12,375 ± 3223

the end of this phase as well as in the subsequent one (phase 4), even though the conditions were theoretically different (i.e., presence and absence of oxygen, respectively). This could suggest that the concentration of oxygen present at the beginning of phase 3 decreased over time until it reached a minimum that corresponded to the concentration in phase 4. This consumption of oxygen in the aqueous solution might limit the cathodic reaction.

Another observation from Fig. 5 is that the corrosion rates in the phases 3 and 4 (approx. 60 µm/year) were higher than in phase 1 (approx. 20 µm/year), although the conditions in terms of temperature, pressure, and oxygen concentration were identical. To investigate if these higher corrosion rates were due either to metal surface effects or to changes in the electrolyte chemistry (related to the history of the 4 stages and the interaction with the environment in phase 2, e.g., exchange of gases), we performed the final experimental phase 5. In this phase, the electrolyte was replaced with a fresh one, identical to phase 1, while the sample was kept unchanged (after having experienced the exposure history of phases 1–4). The results indicated that an influence of the fluid chemistry could be excluded, because the corrosion rates in phase 5 were practically identical to those in phases 3 and 4. Thus, the higher corrosion rates (50–70 µm/year) in phases 3–5 must be related to changes of the metal surface during phases 1 and 2. This will be discussed in "Metal surface changes (roughening, scale formation)" section.

Table 4 compares the R_p values obtained from the LPR and EIS measurements. Here, the LPR data were obtained at the same day and time as the EIS (the difference between the end of the LPR and the beginning of the EIS was about 15 min). In the case of the EIS, the R_p is calculated as the sum of R_{film} and R_{ct} (Table 3) and the error is given. Considering the different time of measurement within a single experimental phase, the R_p values determined with the two techniques differ by a factor 2–3, where EIS generally yields higher R_p than LPR. Nonetheless, the R_p values determined with the two techniques show the same trend going from phase 1 to phase 5. On phase 2, LPR and EIS were almost identical. In the other phases, the lower R_p values obtained from the LPR measurements compared to EIS might be due to the not completely steady state conditions (sweep rate 10 mV/min) (Guyader et al. 2009).

Metal surface changes (roughening, scale formation)

From the impedance spectroscopy results, a corrosion mechanism taking place at the metal surface during the different phases of the measurements can be suggested. The two time constants observed might correspond to the corrosion reaction (R_{ct}, CPE_{dl}) as

Journal : BMCOne 40517 | Dispatch : 9-3-2020 | Pages : 17
Article No : 163 | ☐ LE | ☐ TYPESET
MS Code : | ☑ CP | ☑ DISK

well as to the (porous) iron corrosion products (R_{film}, CPE_{film}). Visible inspection of the metal samples after the tests indeed detected such corrosion product layers. From the values of CPE_{film} (Table 3) and the formula for a capacitance

$$C = \varepsilon_r \cdot \varepsilon_0 \cdot A/d \tag{4}$$

with the relative dielectric constant for iron oxide $\varepsilon_r = 12$ (Stimming and Schultze 1976) and the surface area A of the sample (11 cm^2), the thickness d of the porous oxide layer results in approximately 250 µm. This is in agreement with former studies utilizing surface analysis methods (Vallejo Vitaller et al. 2019) showing that at 200 °C and with the same metal and similar fluid chemistry as in phases 1 and 3–5 of the current work, a protective scale (mainly consisting of hematite) was formed on the metal surface. This scale formation may explain the gradual decrease of corrosion rate that was observed within phase 3. Note that R_{film} (associated to a porous corrosion product layer) was low, indicating a good electrical conductivity. As apparent from the Nyquist and Bode plots, this corrosion product layer likely formed on the metal surface early in the tests (phase 1), and did only marginally change afterward. It is interesting to note that in phase 2, the corrosion rates were substantially increased, which may largely be explained by the higher oxygen concentration in this phase. Interestingly, at the same time, there is also an increase in the double layer capacitance C_{dl} (approx. by a factor 3). This could indicate that the surface roughness of the electrode was increased (roughening due to corrosion attack, which increased the underlying metal surface area). Concerning this capacitance (C_{dl}), Table 3 also shows an increase between the beginning of the tests (phase 1) and the last phases (4 and 5) by a factor of 3, which may again be related to a higher effective steel surface area due to surface roughening. This hypothesis is in agreement with earlier studies showing that corrosion of metals embedded in porous media (here, a porous corrosion product layer) is at the microscopic scale non-uniform and thus leads to surface roughening (Romanoff 1957; Stefanoni et al. 2019). Thus, in summary, the increase in corrosion rate by a factor of 3 between phase 1 (approx. 20 µm/year) and phases 3–5 (approx. 60 µm/year), as observed through electrochemical techniques, may be explained by an increase in effective steel surface area due to surface roughening, as a result of corrosion attack. Thus, the specific (area corrected) corrosion rate in phases 3–5 was 20 µm/year as in phase 1. This means that upon corrosion attack, the surface of the exposed metal becomes rougher, and thus, a higher effective surface area becomes exposed to the electrolyte, where the electrochemical corrosion reactions can occur.

The Bode phase angle plot (Fig. 7b) also showed that the spectra of the five phases had a similar behavior (RQ) at higher frequencies. Regarding the Ohmic resistance (R_s) in phase 2 that was about two times higher than in the other phases (1, 3, 4, 5), the reason for this difference is that the distance between the working electrode with respect to the reference electrode increased due to the opening (and lifting) of the autoclave lid (Fig. 2).

The Bode magnitude plot (Fig. 7a) showed that the impedance of the system increased toward lower frequencies. At 0.01 Hz, the phase 1 had the highest impedance value, the phase 2 had the lowest, and the remaining phases (3, 4, and 5) presented intermediate values. This trend of resistance behavior follows the results obtained with the LPR measurements.

Journal : BMCOne 40517 | Dispatch : 9-3-2020 | Pages : 17
Article No : 163 | ☐ LE | ☐ TYPESET
MS Code : | ☑ CP | ☑ DISK

Implications (for geothermal energy technology)

Operational and maintenance activities in geothermal power plants might have a strong influence on the degradation of the construction materials, and in consequence, on the long-term behavior of the power plant (Schreiber et al. 2016). While planned preventive maintenance is advantageous to collect information concerning the condition of the power plant and to extend its service life, reactive maintenance should be ultimately applied. Therefore, it is important to detect early warnings of damaged equipment because if a component suddenly fails, the operation of the entire power plant needs to be stopped, resulting in higher production costs (Velayutham and Ismail 2018). As shown in the results obtained, shutdown times should be as short as possible, as they might result in the ingress of oxygen into the system and in the (temporary) decrease of temperature. The latter can also occur during the regular operation of the power plant, where the heat in the reservoir becomes gradually depleted over its lifetime. Furthermore, other components of the power plant that handle the hot brines, such as the pipeline system located on the surface between the wellheads and heat exchangers (Fig. 1), are not exempt of corrosion problems (Karlsdottir 2012; Miranda-Herrera et al. 2010). Other types of corrosion, such as crevice corrosion, must be considered when selecting materials for the power plant equipment. The stagnant fluid in the crevices might intensify the local concentration of agents, such as the oxygen in aerated environments (Ellis and Conover 1981; Iberl et al. 2015).

Conclusions

Ensuring durability, while taking into account different possible operational and maintenance issues, is important for the sustainable and cost-effective implementation of geothermal energy as an alternative technology to contribute to the energy supply in the future. Based on the current experimental observations, the following major conclusions can be drawn:

- Two of the most dominant factors influencing the durability of carbon steel in a geothermal power plant in the fluid tested here are the concentration of oxygen and the temperature. A change of these parameters might significantly influence the corrosion rate. Temporary ingress of oxygen and decrease of temperature from 180 to 90 °C (e.g., due to maintenance work) were found to raise the corrosion rate by a factor of more than 5 (from approx. 20 µm/year to > 120 µm/year).
- The corrosion rates of carbon steel were relatively high (110–150 µm/year) in conditions of low temperature (about 90–100 °C) and in presence of oxygen. However, within a few days, the corrosion rate was found to decrease and stabilize around values of 50–70 µm/year, probably due to the formation of a protective corrosion product layer on the metal surface.
- Electrochemical testing (EIS, LPR) in the autoclave by means of an advanced multi-instrument test setup allowed to analyze the corroding system during the different exposure phases. In particular, EIS revealed an increase in capacitance of the double layer by a factor of approx. 3. This increase in capacitance occurred largely during the stage where the metal was exposed to oxygen and thus corroded at the highest rate. Comparing this with the LPR data collected in the five different experimental phases

Journal : BMCOne 40517 | Dispatch : 9-3-2020 | Pages : 17
Article No : 163 | ☐ LE | ☐ TYPESET
MS Code : | ☑ CP | ☑ DISK

suggests that the increase in capacitance was due to an increase in effective corroding steel surface area (as a result of surface roughening due to corrosion attack).

- The experimental work carried out in this contribution implies that changes in exposure conditions (oxygen ingress, temperature)—occurring either in the course of temporary maintenance interventions of geothermal power plants or long-term changes (e.g., thermal gradient reduction of the reservoir)—are important to be considered when designing and operating geothermal power plants. As these environmental changes and their impact on the corrosion state are complex and cannot be generalized, further studies and testing are recommended.

Acknowledgements
Not applicable.

Authors' contributions
All authors designed the research. AVV performed the experiments. All authors contributed in analyzing the data and writing the paper. All authors read and approved the final manuscript.

Funding
The financial support of this project from the Swiss Competence Center for Energy Research–Supply of Electricity (SCCER-SoE) is kindly acknowledged.

Availability of data and materials
All data generated or analyzed during this study are included in this published article. Raw data can be provided upon request.

Competing interests
The authors declare that they have no competing interests.

Author details
[1] Institute for Building Materials (IfB), ETH Zurich, Stefano-Franscini-Platz 3, 8093 Zurich, Switzerland. [2] Department of Chemical and Geological Sciences, University of Cagliari, 09100 Monserrato, CA, Italy.

Received: 5 January 2020 Accepted: 5 March 2020

References

Angst U, Elsener B, Larsen C, Vennesland Ø. Chloride induced reinforcement corrosion: rate limiting step of early pitting corrosion. Electrochim Acta. 2011;56:5877–89.
Anon Guide for geothermal field and plant operation and maintenance, Quito (Ecuador): Latin American Energy Organization (OLADE) & Inter-American Development Bank (IDB). 1994.
API Specification CT. Specification for Casing and Tubing. 8th ed. Washington: API Publishing Services; 2005.
Aristia G, Hoa LQ, Bäßler R. Corrosion of carbon steel in artificial geothermal brine: influence of carbon dioxide at 70 °C and 150 °C. Materials. 2019;12(22):3801.
Atlason R, Oddsson G, Unnthorsson R. Geothermal power plant maintenance: evaluating maintenance system needs using quantitative kano analysis. Energies. 2014;7:4169–84.
Barbier E. Geothermal energy technology and current status: an overview. Renew Sustain Energy Rev. 2002;6:3–65.
Bodmer P, Rybach L. Heat flow maps and deep ground water circulation: examples from Switzerland. J Geodyn. 1985;4:233–45.
Bousselmi L, Fiaud C, Tribollet B, Trik E. "Impedance spectroscopic study of a steel electrode in condition of scaling and corrosion: interphase model. Electrochim Acta. 1999;44(24):4357–63.
Brug G, Van Den Eeden ALG, Sluyters-Rehbach M, Sluyters J. The analysis of electrode impedances complicated by the presence of a constant phase element. J Electroanal Chem Interfacial Electrochem. 1984;176(1–2):275–95.
CEN. EN 13306:2010—maintenance terminology. s.l.: European committee for standardization; 2010.
Clark C, Harto C, Sullivan JL, Wang M. Water use in the development and operation of geothermal power plants (No. ANL/EVS/R-10/5), Argonne, IL (United States): Argonne National Laboratory (ANL). 2010.
Dickson MH, Fanelli M. Geothermal energy: utilization and technology. 1st ed. London: Routledge; 2013.
Ellis PF, Conover MF. Materials selection guidelines for geothermal energy utilization systems. Austin: Radian Corp; 1981.
Farelas F, et al. Evolution of dissolution processes at the interface of carbon steel corroding in a CO_2 environment studied by EIS. Corros Sci. 2010;52(2):509–17.
Guyader A, Huet F, Nogueira RP. Polarization resistance measurements: potentiostatically or galvanostatically? Corrosion. 2009;65(2):136–44.
Hirschberg S, Wiemer S, Burgherr P. Energy from the earth: deep geothermal as a resource for the future? Zurich (Switzerland): vdf Hochschulverlag AG, ISBN 978-3-7281-3654-1. 2015.

Journal : BMCOne 40517 | Dispatch : 9-3-2020 | Pages : 17
Article No : 163 | ☐ LE | ☐ TYPESET
MS Code : | ☑ CP | ☑ DISK

Iberl P, Alt NSA, Schluecker E. Evaluation of corrosion of materials for application in geothermal systems in Central Europe. Mater Corros. 2015;66:733–55.

Jones D. Principles and prevention of corrosion. Upper Saddle River: Prentice-Hall; 1996.

Karlsdottir SN. Corrosion, scaling and material selection in geothermal power production. In: Sayigh A, editor. Comprehensive renewable energy. Amsterdam: Elsevier; 2012. p. 241–59.

Landolt D. Corrosion and surface chemistry of metals. s.l.: EPFL press; 2007.

Lu S. A global review of enhanced geothermal system (EGS). Renew Sustain Energy Rev. 2018;81:2902–21.

Lund J, Boyd T. Direct utilization of geothermal energy 2015 worldwide review. Geothermics. 2016;60:66–93.

Miranda-Herrera C, Sauceda I, González-Sánchez J, Acuña N. Corrosion degradation of pipeline carbon steels subjected to geothermal plant conditions. Anti-Corros Methods Mater. 2010;57(4):167–72.

Mundhenk N, et al. Corrosion and scaling as interrelated phenomena in an operating geothermal power plant. Corros Sci. 2013;70:17–28.

Mundhenk N, et al. Corrosion of carbon steel and the passivating properties of corrosion films formed under high-PT geothermal conditions. Sci Total Environ. 2019;677:307–14.

Nogara J, Zarrouk SJ. Corrosion in geothermal environment Part 2: metals and alloys. Renew Sustain Energy Rev. 2018a;82:1347–63.

Nogara J, Zarrouk SJ. Corrosion in geothermal environment: part 1: Fluids and their impact. Renew Sustain Energy Rev. 2018b;82:1333–46.

Ochieng L. Overview of geothermal surface exploration methods, Lake Bogoria and Lake Naivasha (Kenya): Presented at Short Course IX on Exploration for Geothermal Resources organized by UNU-GTP, GDC and KenGen. 2014.

Olasolo P, Juarez MC, Morales MP, Liarte IA. Enhanced geothermal systems (EGS): a review. Renew Sustain Energy Rev. 2016;56:133–44.

Revie R, Uhlig H 4th. Corrosion and corrosion control: an introduction to corrosion science and engineering. New York: Wiley; 2008.

Romanoff M. Underground corrosion. Washington, DC: US: Government Printing Office. 1957.

Schreiber S, Lapanje A, Ramsak P, Breembroek G. Operational issues in geothermal energy in Europe: status and overview. Reykjavik (Iceland): Geothermal ERA NET; 2016.

Sonney R, Vuataz F. Properties of geothermal fluids in Switzerland: a new interactive database. Geothermics. 2008;37:496–509.

Stefanoni M, Angst U, Elsener B. Kinetics of electrochemical dissolution of metals in porous media. Nat Mater. 2019;18(9):942–7.

Stern M, Geary AL. Electrochemical polarization I A theoretical analysis of the shape of polarization curves. J Electrochem Soc. 1957;104(1):56–63.

Stimming U, Schultze J. The capacity of passivated iron electrodes and the band structure of the passive layer. Ber Bunsenges Phys Chem. 1976;80(12):1297–302.

Sullivan G, Pugh R, Melendez A, Hunt W, Release 3.0, Operations & Maintenance. Best practices. A Guide to Achieving Operational Efficiency., s.l.: Pacific Northwest National Laboratory for the Federal Energy Management Program, US Department of Energy. 2010.

Swiss Federal Office of Energy, n.d. Energy Strategy 2050 once the New Energy Act is in Force. http://www.bfe.admin.ch/energiestrategie2050/. Accessed 3 January 2019.

Vallejo Vitaller A, Angst U, Elsener B. Corrosion Behaviour of L80 Steel Grade in Geothermal Power Plants in Switzerland. Metals. 2019;9(3):331.

Vallejo Vitaller A, Angst U, Elsener B. A setup for electrochemical corrosion testing at elevated temperature and pressure. Measurement. 2020;155:107537.

Velayutham P, Ismail F. A Review on Power Plant Maintenance and Operational Performance. 2018. vol. 225, p. 05003.

Wyss R, Link K. Actual Developments in Deep Geothermal Energy in Switzerland. Melbourne (Australia). 2015.

Publisher's Note

Springer Nature remains neutral with regard to jurisdictional claims in published maps and institutional affiliations.

Journal : BMCOne 40517	Dispatch : 9-3-2020	Pages : 17
Article No : 163	☐ LE	☐ TYPESET
MS Code :	☑ CP	☑ DISK

Journal:	**40517**
Article:	**163**

Author Query Form

Please ensure you fill out your response to the queries raised below and return this form along with your corrections

Author Proof

Dear Author

During the process of typesetting your article, the following queries have arisen. Please check your typeset proof carefully against the queries listed below and mark the necessary changes either directly on the proof/online grid or in the 'Author's response' area provided below

Query	Details Required	Author's Response
AQ1	Article title: Kindly check and confirm the edit made in the article title.	
AQ2	Author names: Please confirm if the author names are presented accurately and in the correct sequence (given name, middle name/initial, family name). Author 1 Given name: Ana Vallejo, Last name: Vitaller:	